BIOCHEMISTRY
including biophysical chemistry & molecular biology

Article

pubs.acs.org/biochemistry

Relationship between Structural Flexibility and Function in the C-Terminal Region of the Heparin-Binding Domain of $VEGF_{165}$

Ki-Woong Jeong, Min-Cheol Jeong, Bonghwan Jin, and Yangmee Kim*

Department of Bioscience and Biotechnology and Bio/Molecular Informatics Center, Institute of KU Biotechnology, Konkuk University, Seoul 143-701, Korea

Supporting Information

ABSTRACT: Vascular endothelial growth factor (VEGF) is an angiogenic protein with neurotrophic and neuroprotective effects. Previously, we reported that triamterene (Trm) inhibits VEGF−amyloid β (Aβ) interactions without affecting other biological activities of VEGF or Aβ [Jeong, K.-W., et al. (2011) *Biochemistry 50*, 4843−4854]. We further showed that molecular motions in the N-terminal disordered loop region of the heparin-binding domain (HBD) are important for interaction with Trm. To investigate the importance of motion at the C-terminal domain of HBD, we constructed a binding model of HBD with heparin octasaccharide (HOS) based on measurements of chemical shift changes and docking studies. Furthermore, the dynamic properties of the HBD−HOS and HBD−Trm−HOS complexes were assessed by measuring spin relaxation rates. The results showed that the HOS-binding site is composed of two basic clusters consisting of side chains of residues R13, R14, and K15 and residues K30, R35, and R49. When HOS binds, values for the heteronuclear nuclear Overhauser effect near HOS-binding sites increased dramatically. CPMG (Carr−Purcell−Meiboom−Gill sequence) experiments as well as an R_2 relaxation experiment were undertaken to understand millisecond time-scale motions in HBD. There is large relaxation dispersion of residues at Trm- and HOS-binding sites in free HBD. C-Terminal residues such as S34, C48, and D51 near the HOS-binding sites continued to exhibit slow conformational motions in the HBD−Trm complex, while those slow motions disappeared in the bound conformation of HBD with HOS. Collectively, our results demonstrate that the inherent structural flexibilities of the C-terminal region of the HBD are important in the heparin binding process and that Trm does not inhibit VEGF−heparin interactions necessary for the biological activities of VEGF.

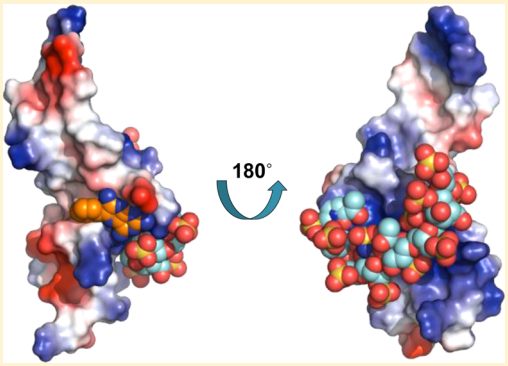

Vascular endothelial growth factor (VEGF) is an essential growth factor that plays a key role in most aspects of vascular development and function. VEGF is also a key regulator of pathological angiogenesis, which is involved in cancer, rheumatoid arthritis, and retinopathy.[1−5] VEGF is a disulfide-linked homodimer that is expressed as different isoforms ranging in size from 121 to 206 residues in humans ($VEGF_{121}$, $VEGF_{165}$, $VEGF_{189}$, and $VEGF_{206}$) through alternate mRNA splicing.[6,7] VEGF variants are variably expressed in different tissues, but all mediate mitogenic actions, regulate vascular permeability in endothelial cells, and are the main regulators of hypoxia and tumor-induced angiogenesis.[8] To date, the best-characterized VEGF isoform is the 165-amino acid form ($VEGF_{165}$). Structural studies of VEGF have been performed by a number of researchers. Muller et al. was the first to determine the three-dimensional (3D) structure of VEGF in 1997 using X-ray crystallography.[9] $VEGF_{165}$ consists of two domains: a receptor-binding domain, which is present in all four isoforms of VEGF, and a short C-terminal heparin-binding domain (HBD) that distinguishes $VEGF_{165}$ from the other isoforms.[10]

Heparin binding is important for the activities of VEGF, regulating mitogenic activity, tube formation, and VEGF−receptor binding.[11−13] As shown in Figure 1B, the HBD contains two clearly defined subdomains: the N-terminal subdomain (residues 1−29) and the C-terminal subdomain (residues 29−55).[14,15] The HBD of VEGF, which has no significant sequence or structural similarities to other known proteins,[1,11,14] is highly flexible because of its lack of a hydrophobic core; its folding appears to be dominated by four disulfide bonds.[14] It also has a highly basic surface that is thought to serve as a heparin-binding site.[14]

$VEGF_{165}$ is a heparin-binding growth factor, and the binding of $VEGF_{165}$ to cell surface receptors on vascular endothelial cells is strongly modulated by cell surface-associated heparin-like molecules. Heparin is a highly sulfated polysaccharide consisting of a repeating disaccharide structure like that found in other glycosaminoglycans. Heparin exhibits a high degree of heterogeneity because of variations in its size and general level of sulfation. Recent *in vitro* and *in vivo* studies designed to test the efficacy of targeting relevant angiogenic growth factors as a strategy for inhibiting tumor angiogenesis have shown promising primary results for therapies using heparin- and

Received: August 24, 2013
Revised: November 22, 2013
Published: November 25, 2013

   dx.doi.org/10.1021/bi4011682 | *Biochemistry* 2013, 52, 8823−8832

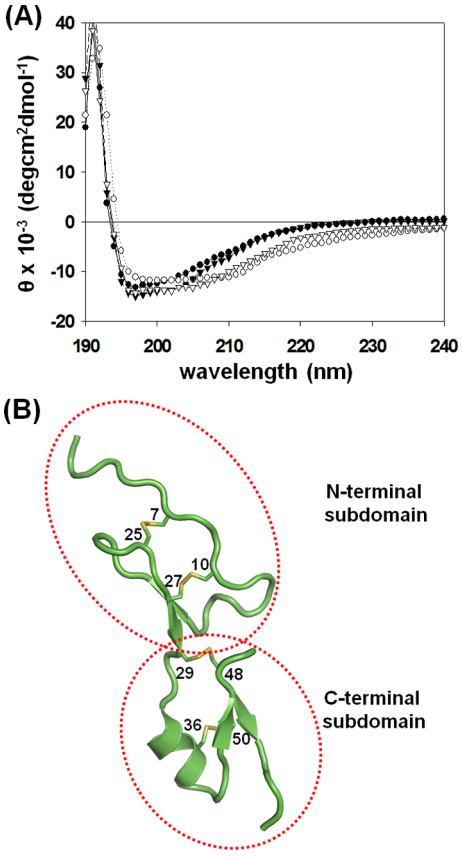

Figure 1. (A) Circular dichroism spectra of free HBD (●) and HBD−Trm (○), HBD−HOS (▼), and HBD−Trm−HOS complexes (▽) in 25 mM sodium acetate (pH 5.5) at 300 K. (B) Ribbon structure of the HBD showing secondary structural elements and four disulfide bonds (yellow). The N-terminal subdomain (residues 1−29) and the C-terminal subdomain (residues 29−55) are encircled.

heparin sulfate (HS)-based oligosaccharides.[16−19] These compounds competitively bind to heparin-binding growth factors, preventing their interaction with cell surface heparin sulfate proteoglycans (HSPGs) and cytokine receptors, thereby inhibiting angiogenesis.[16] The potential therapeutic benefit of low-molecular weight heparin (LMWH), a highly sulfated HS, was observed in preclinical models, where it acted as an antiangiogenic, antimetastatic, and anti-inflammatory agent.[20−23] LMWH, for example, has been demonstrated to potently inhibit FGF-2- and VEGF-mediated human microvascular endothelial cell proliferation.[24,25] Recently published evidence has implicated HS oligosaccharides in the suppression of endothelial cell migration, tube formation, and signaling induced by $VEGF_{165}$ and FGF-2.[26] Linhardt and colleagues also have determined that the minimal size of heparin oligosaccharides for binding to $VEGF_{165}$ and the HBD under physiological conditions is an octasaccharide.[19]

The structure of the HBD has been studied by nuclear magnetic resonance (NMR) spectroscopy.[14,15] The N-terminal region, containing two disulfide bonds (C7−C25 and C10−C27), is composed of a disordered region from S11 to L17, and a single two-stranded antiparallel β-sheet structure encompassing F18−D21 and K26−C29.[14] The C-terminal region, which also has two disulfide bonds (C29−C48 and C36−C50), is well-ordered and contains a short α-helix from D33 to A38 packed against a two-stranded antiparallel β-sheet structure consisting of E42−N44 and R49−D51.[14] In our previous study, we showed that molecular motions in the N-terminal disordered loop region of the HBD are important for interactions with the inhibitor triamterene (Trm).[27] We proposed that Trm recognizes the slow motions in the N-terminal disordered loop region of HBD. Interestingly, residues at the C-terminus of the HBD still showed slow motions in the HBD−Trm complex. We also found that Trm inhibited the binding of amyloid β (Aβ) to VEGF with an IC_{50} of 50 μM but did not inhibit binding of VEGF to the VEGF receptor KDR (kinase insert domain receptor, VEGFR2), implying that Trm does not affect the biological activity of VEGF.[27] Here, we investigated the flexibilities at the C-terminal region of the HBD and found that the inherent structural flexibilities of this region are important in the heparin recognition process.

MATERIALS AND METHODS

Expression and Purification of the HBD. VEGF cDNA was previously cloned into a pRSET-A vector (Invitrogen, Carlsbad, CA) containing a T7 promoter and an ampicillin-resistance cassette. The ^{15}N-labeled HBD was produced from the *Escherichia coli* transformed by the recombinant plasmid in 1 L of M9 minimal medium supplemented with ampicillin and 1 g/L $^{15}NH_4Cl$ (Cambridge Isotope Laboratories, Cambridge, MA).[28] The HBD was purified according to a previously published method.[14] The correctly folded, His-tagged HBD was purified by affinity chromatography using a HiTrap chelating column. The His tag was removed from the HBD by cleavage with enterokinase (Invitrogen), and final purification was achieved by cation exchange chromatography using a HiTrap SP FF column (GE Healthcare, Uppsala, Sweden) that was eluted with a 0 to 1 M NaCl gradient. Samples for NMR were resuspended in 25 mM sodium d_3-acetate buffer (pH 5.5) containing 0.02% NaN_3.

Circular Dichroism Measurements of the HBD. Circular dichroism (CD) experiments were performed using a J810 spectropolarimeter (Jasco, Tokyo, Japan) with a 1 mm path-length cell. The CD spectra of the free HBD, the HBD with Trm or heparin octasaccharide (HOS), and the HBD with both Trm and HOS in 25 mM sodium acetate buffer (pH 5.5) at 27 °C were recorded at 0.1 nm intervals from 190 to 250 nm. The HOS was purchased from iduron [Manchester, U.K. (http://www.iduron.co.uk)]. The peptide concentration was 20 μM for all CD experiments. For each spectrum, the data from 10 scans were averaged and smoothed using J810 software. CD data were expressed as the mean residue ellipticity [θ] in degrees square centimeters per decimole.

NMR Experiments and Assignment. All NMR experiments were performed at 27 °C on a Bruker Avance 500 or 800 MHz spectrometer at the Korea Basic Science Institute (Ochang, Korea). Internal 2,2-dimethyl-2-silapentane-5-sulfonate (DSS) was used as a chemical shift reference of NMR spectra. The ^{15}N-labeled HBD in 25 mM sodium acetate buffer (pH 5.5) was in 0.4 mM solutions in 0.3 mL of a 9:1 (v/v) H_2O/D_2O mixture for heteronuclear single-quantum coherence (HSQC) analysis. Chemical shift changes in the $^1H-^{15}N$ spectra of the HBD were obtained by titration with HOS. The magnitude of the chemical shift perturbation and changes in the intensities upon binding HOS were utilized to map binding site residues in the HBD. Two-dimensional NOESY experiments were also performed to identify intermolecular NOEs between the HOS and HBD. Mixing times of 250, 400, 600, and 800 ms were used in collecting NOE spectra for both free and HOS complex samples.

dx.doi.org/10.1021/bi4011682 | *Biochemistry* 2013, 52, 8823−8832

Construction of a Binding Model of the HBD−Trm Complex and HOS. A molecular docking study and molecular dynamics (MD) simulations were conducted to construct binding models of the HOS and HBD complex as well as HOS and the HBD−Trm complex.[27] Computations were performed on a Windows platform using CDOCKER, a CHARMm-based MD method for ligand docking, in Discovery Studio (DS) modeling (Accelrys Inc., San Diego, CA).[29−31] The docking program was used to find the initial configurations for HOS with the HBD and HOS with HBD−Trm complex structures. The initial structural model of the HOS was built via DS modeling based on its NMR solution structure (Protein Data Bank entry 1HPN).[32] Docking experiments were performed using a heparin octamer. The repeating disaccharide unit of heparin was composed of a fully N-, 2-O-, and 6-O-sulfated iduronic acid [IdoA(2S)] and 6-O- and N-sulfated glucosamine [GlcNS(6S)]. For docking of HOS, all sulfate groups were allowed to rotate freely. The Input Site Sphere parameter specifies a sphere around the center of the binding site, where the CDOCKER experiment is to be performed. The center of the sphere was used in the CDOCKER algorithm for initial ligand placement. The MD-simulated annealing process was performed using a rigid protein and flexible ligand. The MD simulation was conducted using the final docking structures with the Standard Dynamics Cascade Protocol in DS modeling. For initial minimization, the steepest descent method was employed to a 0.1 kcal mol^{-1} $Å^{-1}$ root-mean-square (rms) energy gradient and followed by the conjugate gradient method until the final convergence criterion reached a 0.001 kcal mol^{-1} $Å^{-1}$ RMS gradient. Then the whole system was heated from 50 to 300 K in 2 ps and equilibrated at 300 K for 100 ps. One hundred conformations were collected in a 20 ps production phase at 300 K.

Investigation of Backbone Dynamics by NMR. NMR studies utilized the resonance assignments of the HBD reported previously by Fairbrother et al.[14] All relaxation experiments were conducted on 500 MHz instruments. Protein samples for all relaxation measurements were dissolved at a concentration of ∼0.7 mM in 25 mM sodium acetate buffer (pH 5.5) prepared using 10% D_2O and 90% H_2O (at 27 °C). Ambiguities in resonance assignments of the HOS-bound HBD and HOS−Trm-bound HBD were resolved by recording $^1H-^{15}N$ nuclear Overhauser effect spectroscopy (NOESY)-HSQC and $^1H-^{15}N$ total correlation spectroscopy (TOCSY)-HSQC.[33,34] NMR spin relaxation experiments were performed using previously published gradient-selected, sensitivity-enhanced pulse sequences.[35−37] The longitudinal (R_1) spin relaxation rates were measured with relaxation delays of 0.002 (twice), 0.045, 0.1, 0.2, 0.315 (twice), 0.55, 0.8, and 1.0 s. The transverse (R_2) relaxation rates were obtained with total relaxation delays of 0.0 (twice), 0.0176, 0.0352, 0.0528 (twice), 0.068, 0.1145, 0.184, and 0.284 s. For R_2 measurements, temperature-compensating ^{15}N 180° pulses were applied during the recycle delay.[38] The heteronuclear cross-relaxation rate was obtained from nuclear Overhauser effect (NOE) experiments by interleaving pulse sequences with and without proton saturation. The recycle delay and proton saturation time in the heteronuclear NOE (hNOE) measurement were 4.5 and 3.0 s, respectively. All relaxation spectra were acquired with the ^1H carrier set coincident with the water resonance and the ^{15}N frequency set to 118 ppm; spectral widths were 5498 and 1612 Hz in the t_2 and t_1 dimensions, respectively, with 2048 and 200 complex points in each dimension. A recycle delay of 2.5 s was used in all R_1 and R_2 relaxation experiments. NMR data were processed with NMRPipe and visualized with Sparky.[39,40] Typically, 35.0 μs ^{15}N 90° pulse widths could be achieved with an xyz-gradient-equipped Bruker TXI (^1H, ^{13}C, ^{15}N) probe.

The hNOE was determined from the ratio of peak heights for experiments with and without proton saturation pulses. R_1 and R_2 values were determined by fitting the peak heights using Curvefit available at the Palmer group's homepage (http://biochemistry.hs.columbia.edu/labs/palmer/software/curvefit.html).

Constant time relaxation-compensated Carr−Purcell−Meiboom−Gill (CPMG) experiments were performed under the following conditions. For the sample at 0.7 mM free HBD and HBD complex with HOS or Trm and both HOS and Trm, spectra were recorded on the Bruker Avance 500 MHz spectrometer.[41] Relaxation dispersion spectra were recorded as a series of 12 2D data sets with CPMG field strengths, υ_{cp}, of 50, 75, 100, 125, 150 (twice), 200, 250, 300, 400, 500 (twice), 700, and 1000 Hz, and reference spectra were recorded by omitting the CPMG intervals in the pulse sequence. Each 2D spectrum was recorded as a complex data matrix comprised of 192 × 1024 points. Twenty-four scans or free induction decays were recorded using a constant time delay of 40 ms and a recycle delay of 2.0 s, resulting in a net acquisition time of approximately 3 h per data set. The intensities of cross-peaks were then converted into decay rates, R_2^{eff}, for a given υ_{cp}.[42]

Isothermal Titration Calorimetry (ITC). ITC experiments were performed on a high-precision VP-ITC instrument (Microbial Inc., Northampton, MA) at 25 °C. All samples were dissolved in 25 mM sodium acetate buffer (pH 5.5) and degassed before the measurement. The HOS at a concentration of 0.5 mM (volume of 300 μL) was injected into the calorimetric cell containing 0.3 mM (volume of 300 μL) HBD or HBD−Trm complex. Also, the Trm at a concentration of 0.5 mM was injected into the calorimetric cell containing 0.3 mM HBD or HBD−HOS complex. Exhaustive cleaning of the cells was undertaken before each experiment. The calorimetric titration curve for ligand was determined by titrating ligand with protein. After thermal equilibration, the typical titration involved injections of protein into the sample cell containing ligand every 4 min with constant stirring at 250 rpm. The heat evolved after each ligand injection was obtained from the integral of the calorimetric signal.

RESULTS

CD Measurements of the HBD Complexed with HOS and Trm. The CD spectrum of the free HBD as shown in Figure 1A shows a negative band at approximately 195−200 nm, indicating that the HBD does not have stable secondary structures. We previously confirmed on the basis of CD measurements that the β-sheet structure of the HBD is stabilized by complexation with Trm. As shown in Figure 1B, the tertiary folding of the HBD might be maintained by four disulfide bonds (C7−C25, C10−C27, C29−C48, and C36−C50) present in this domain. Here, we investigated the effect of HOS binding on the secondary structure of the HBD by analyzing CD spectra. As shown in Figure 1A, compared to the HBD−Trm complex, the addition of HOS did not change the CD spectrum of the HBD much compared to that of Trm, implying that HOS did not have a significant influence on the secondary structure of the HBD, while Trm stabilized the secondary structures of the HBD. These results were confirmed

dx.doi.org/10.1021/bi4011682 | Biochemistry 2013, 52, 8823−8832

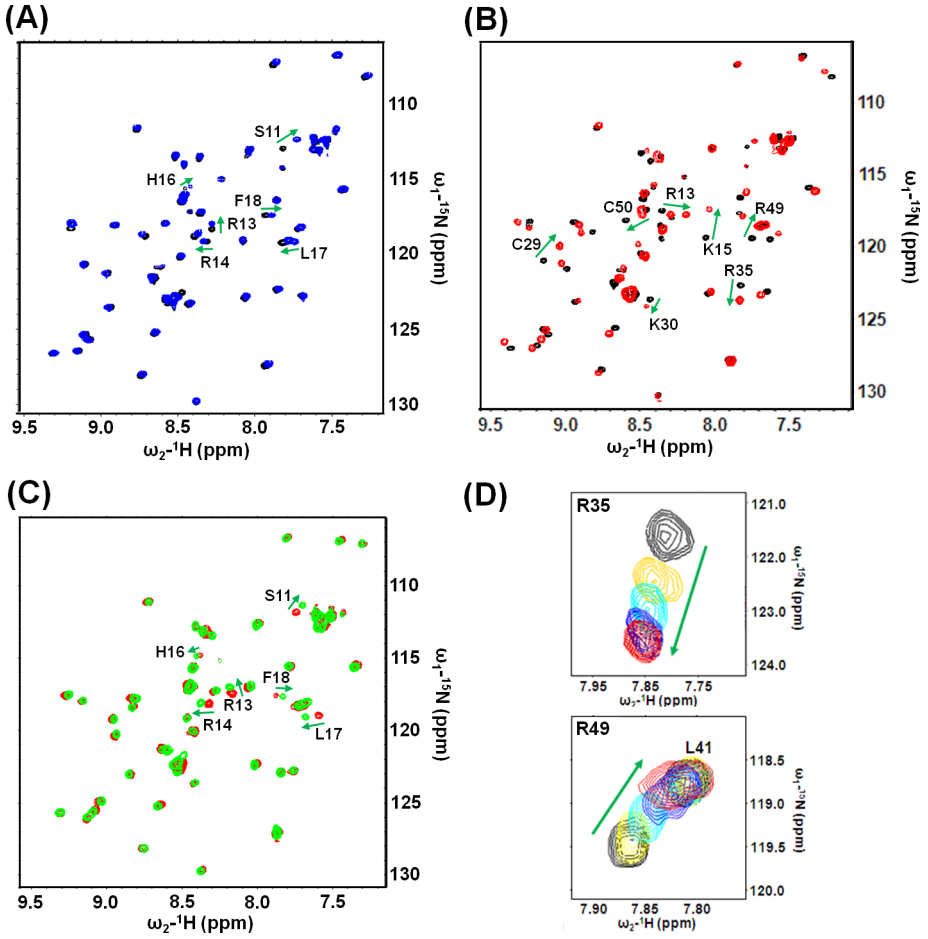

Figure 2. (A) Overlay of HSQC spectra of the free HBD (black) and the Trm-bound HBD (blue). (B) Overlay of HSQC spectra of the free HBD (black) and the HOS-bound HBD (red). The HBD:HOS molar ratio was 1:1. (C) Overlay of HSQC spectra of the HOS-bound HBD and the Trm−HOS complex-bound HBD (green). (D) Peak traces for HOS titration in $^{1}H-^{15}N$ HSQC spectra. 2D spectra show the signal changes of 0.4 mM HBD (red) with titration of HOS at HOS:HBD ratios of (a) 0:1 (black), (b) 0.3:1 (yellow), (c) 0.5:1 (sky blue), (d) 0.7:1 (blue), and (e) 1:1. Shifts in the paths of peaks are denoted with green arrows.

by the chemical shift index of $C_{\alpha}H$ as shown in Figure S1 of the Supporting Information. The chemical shift index of $C_{\alpha}H$ of the free HBD is very similar to those of the HBD−HOS complex, but the HBD−Trm and HBD−Trm−HOS complexes have more stabilized secondary structures and have longer second β-sheet structures compared to those of the free HBD and the HBD−HOS complex.

Chemical Shift Perturbations of the HBD upon HOS Binding. A docking model of heparin/HS heptasaccharide and the HBD has been reported by Robinson et al. using molecular modeling.[43] They predicted that the oligosaccharide lies in a shallow groove consisting of basic residues R14, H16, and K30 on the N-terminal side and R35, R39, and R49 on the C-terminal side. A site-directed mutagenesis study of the HBD by Krilleke and colleagues further showed that residues R13, R14, and R49 are critical for heparin binding and interaction with VEGF receptors.[44]

We observed large chemical shift perturbations for S11, R13, L17, and F18 residues in Trm titration experiments (Figure 2A). To determine the HOS-binding site of the HBD, we performed HOS titration experiments and compared the backbone ^{1}H and ^{15}N chemical shifts in $^{1}H-^{15}N$ HSQC spectra of the HBD in the presence and absence of HOS. Overlays of the $^{1}H-^{15}N$ HSQC spectra of the free HBD and the HOS−HBD complex (HBD:HOS molar ratio of 1:1) are shown in Figure 2B, and the bar graph demonstrating the chemical shift perturbation is shown in Figure S2 of the Supporting Information. Using chemical shift perturbation data, we found that large chemical shift perturbations were clustered in two regions, R13, R14, and K15 and K30, R35, and R49, containing the positively charged residues lysine and arginine. From this, we concluded that these residues facilitate the binding of HOS through direct interaction and/or conformational rearrangements remote from the binding interface. Figure 2D shows the peak traces of R35 and R49 for HOS titration in $^{1}H-^{15}N$ HSQC. The NMR signals gradually shifted in a single direction with the addition of HOS, indicating that the rate of exchange of ligand between the unbound and bound states is faster than the NMR time scale. These results imply that the interaction of HBD with HOS is mediated by basic residues, results consistent with the earlier biochemical study by Robinson et al.[43] To investigate the influence of Trm on the binding of HOS to the HBD, we added Trm to the HBD−HOS complex. A comparison of panels A and C of Figure 2 shows that only Trm-binding residues exhibited chemical shift changes in the HBD−HOS complex, implying that Trm does not affect the binding of HOS to the HBD. To investigate whether Trm binding affects the binding affinity of HOS for the HBD, we measured the binding affinity of HOS for the HBD or the HBD−Trm complex using ITC. As shown in Figure 3, the

dx.doi.org/10.1021/bi4011682 | Biochemistry 2013, 52, 8823−8832

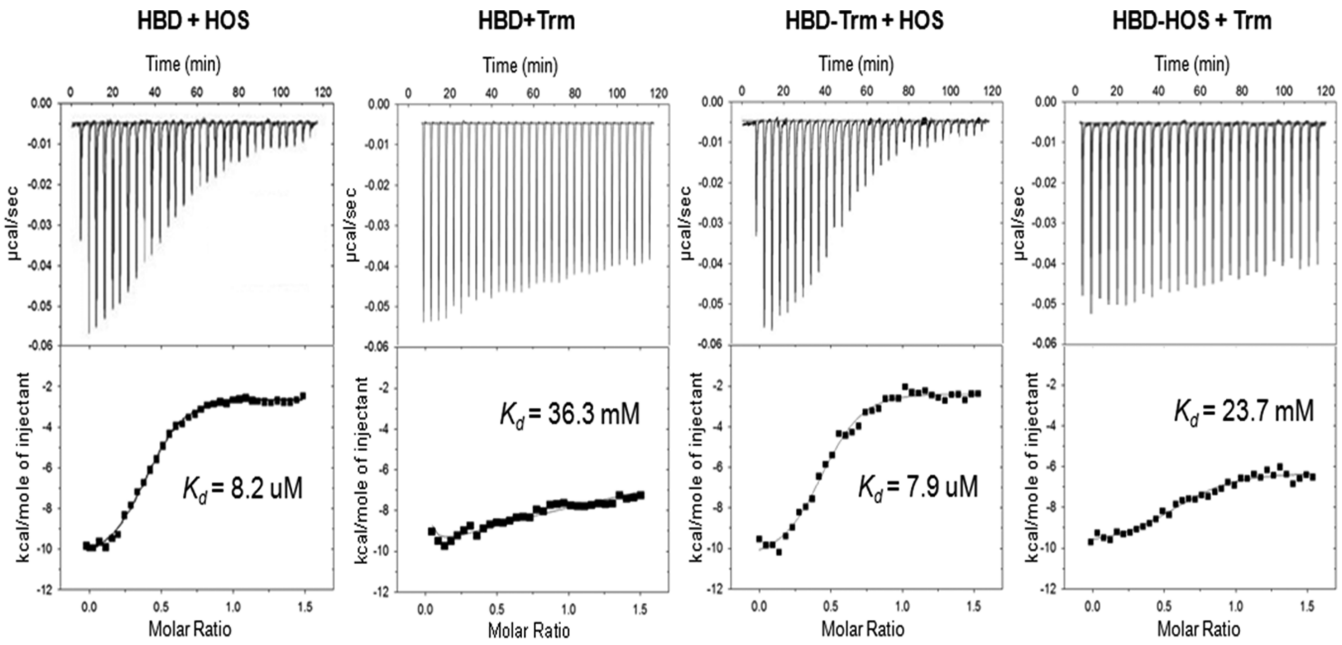

Figure 3. ITC data for binding of HOS and/or Trm to the HBD in 25 mM sodium acetate buffer (pH 5.5).

K_d of HOS for the HBD is 8.2 μM and that for the HBD−Trm complex 7.9 μM, implying that Trm binding does not affect the binding affinity of HOS for the HBD. Also, the K_d of Trm for the HBD is 36.3 mM and that for the HBD−HOS complex 23.7 mM, implying that HOS binding does not affect the binding affinity of Trm for the HBD much, either.

Solution NMR Experiments. We next compared the dynamic properties of the free HBD and the HBD−Trm, HBD−HOS, and HBD−Trm−HOS complexes. The results of spin relaxation experiments with the free HBD and the HBD−Trm, HBD−HOS (HBD:HOS molar ratio of 1:1), and HBD−Trm−HOS complexes are compared in Figure 4. The average (10% trimmed) R_1, R_2, and hNOE values for the free HBD were 2.41 ± 0.023, 7.17 ± 0.13 s^{-1}, and 0.61 ± 0.010 unit, respectively, whereas the corresponding values for the HOS-bound HBD were 2.37 ± 0.066, 8.69 ± 0.42 s^{-1}, and 0.71 ± 0.033 unit, respectively. The average R_2/R_1 ratio for the free HBD was 2.96 ± 0.13, whereas that for the HOS-bound HBD was 3.67 ± 0.43. The HOS-bound HBD has a greater R_2/R_1 ratio than free HBD does because of its higher molecular weight. For R_2, this difference is highly significant, but R_1 is similar in all four cases. This comparatively large increase in R_2 and small decrease in R_1 are expected from the increase in molecular weight upon binding of a ligand to the HBD. Correlation times for the HBD and the HBD−Trm, HBD−HOS, and HBD−Trm−HOS complexes were 5.34 ± 0.01, 5.37 ± 0.02, 6.34 ± 0.02, and 6.51 ± 0.03 ns, respectively, and they correspond to the relative sizes of these molecules, too. In all cases, the R_2 values of residues in the presence of ligand were greater than that of the free HBD except for residues showing large R_2 values (>10 s^{-1}) due to contributions from conformational exchange (R_{ex}) of the protein on micro-second-to-millisecond time scales. In the free HBD, many residues (S11, R13, H16, D21, T24, C25, C27, S34, Q40, N44, and C48) showed R_2 values significantly greater than 10 s^{-1}. The HBD contains four proline residues (6, 9, 22, and 53) and four disulfide bonds (7−25, 10−27, 29−48, and 36−50). We have reported that these large R_2 values (>10 s^{-1}) might be due to loop motion, *cis-trans*-proline isomerization, or disulfide bond isomerization.[27] In the HBD−Trm complex, only R_2 values of the binding loop region from S11 to F18 were dramatically decreased. However, in the HOS−HBD complex, decreases in the extents of conformational exchange of S11 (16.62 to 11.40 s^{-1}), R13 (12.75 to 7.88 s^{-1}), H16 (11.30 to 8.81 s^{-1}), D21 (18.25 to 10.89 s^{-1}), and T24 (11.45 to 9.63 s^{-1}) at the N-terminus as well as C25 (15.41 to 8.82 s^{-1}), C27 (11.00 to 8.49 s^{-1}), S34 (13.47 to 8.82 s^{-1}), Q40 (11.57 to 9.11 s^{-1}), N44 (12.92 to 7.99 s^{-1}), and C48 (12.28 to 10.41 s^{-1}) at the C-terminus were observed. In the HBD−Trm−HOS complex, only D21 and N44 residues showed R_2 values of >10 s^{-1}. This implies that the extent of conformational exchange is reduced dramatically upon HOS and Trm binding and suggests that motions of residues in the disordered loop region at N- or C-terminal regions in the HBD may be essential for ligand and/or inhibitor binding.

The residues at both termini in the free HBD and all HBD complexes exhibited very low hNOE values because of their flexibilities. The average hNOE value was 0.43 for the free HBD, which increased to 0.58 for the HOS-bound form. We found that hNOE values of residues at the Trm-binding site (S11−F18) were dramatically increased by the binding of Trm. In the case of the HOS-bound form, substantial increases in hNOE values were observed for residues R13 (0.53 to 0.76), R14 (0.55 to 0.64), and K15 (0.62 to 0.74) in the N-terminal loop region. Notably, at the C-terminal region (residues 30−55), these values for most residues in the presence of HOS (average hNOE of 0.75 ± 0.030) were higher than those observed in both free (average hNOE of 0.62 ± 0.010) and Trm-bound (average hNOE of 0.65 ± 0.012) forms. These results imply that HOS mainly binds to the C-terminal region in addition to residues R13, R14, and K15 in the N-terminal region. In the HBD−Trm−HOS complex, hNOE values for both the Trm-binding region (0.81 ± 0.034) and the C-terminal region (0.78 ± 0.028) were much higher than those of the free form, implying that Trm and HOS independently bind to the HBD and contribute to its stabilization.

To investigate microsecond-to-millisecond motions in the HBD, we tested the free HBD and the HBD−Trm, HBD−

dx.doi.org/10.1021/bi4011682 | *Biochemistry* 2013, 52, 8823−8832

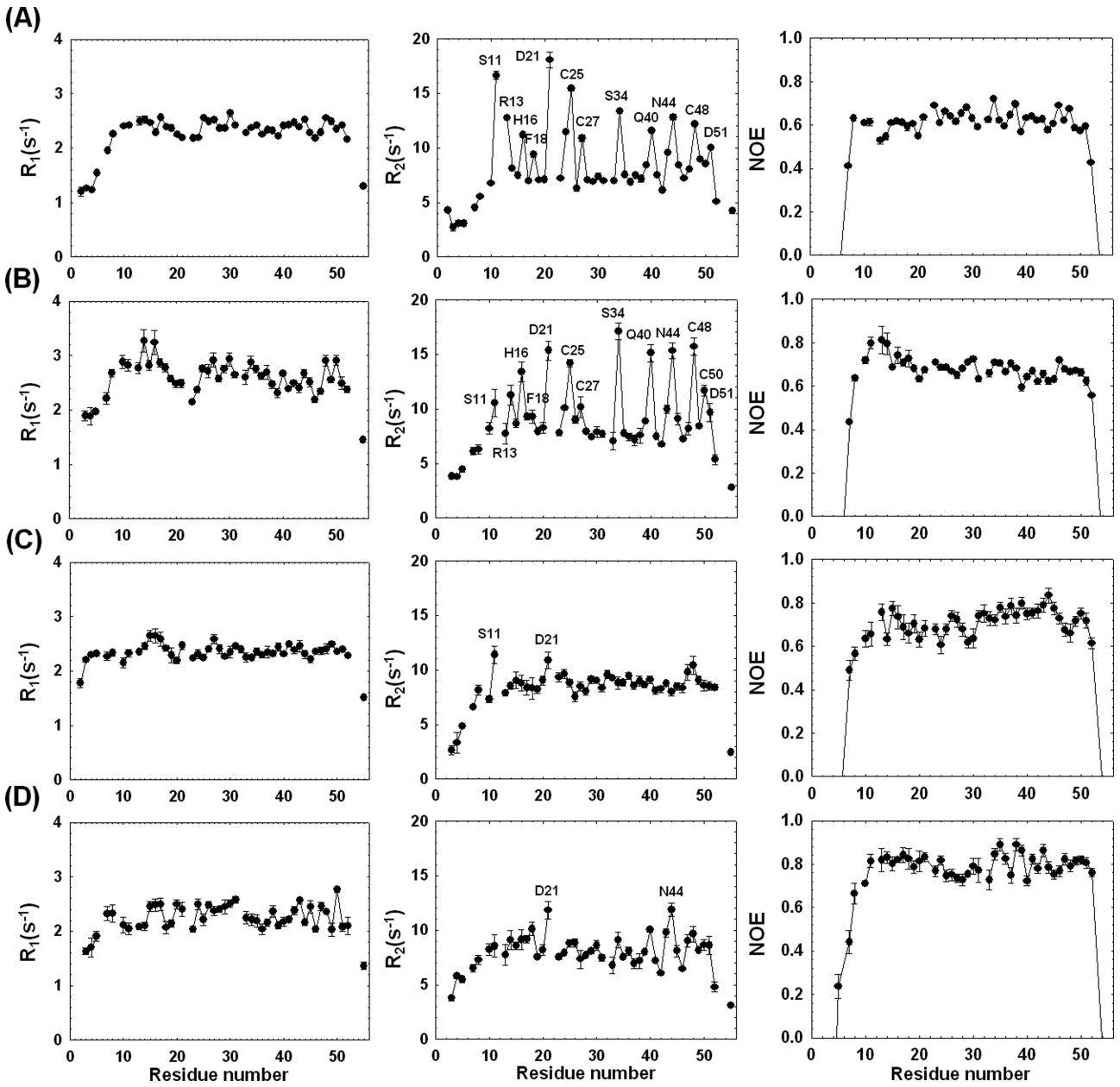

Figure 4. Comparison of R_1, R_2, and hNOE values for (A) the free HBD and the (B) HBD−Trm, (C) HBD−HOS, and (D) HBD−Trm−HOS complexes at pH 5.5. In the case of hNOE data, N-terminal residues 1−5 and C-terminal residue 55 exhibited negative values.

HOS, and HBD−Trm−HOS complexes in CPMG experiments. In Figure 5A−D, the differences in R_2^{eff} values are plotted as a function of amino acid sequence because chemical exchange at the protein backbone is evident from these differences measured at long (ν_{cp} = 50 Hz) and short (ν_{cp} = 1000 Hz) interpulse delays. ^{15}N CPMG relaxation dispersion [ΔR_2^{eff} (ν_{cp}) = R_2^{eff} (ν_{cp}, 50 Hz) − R_2^{eff} (ν_{cp}, 1000 Hz)] revealed that binding of HOS reduced slow time-scale motion, dramatically decreasing the R_{ex} values of the binding epitope while binding of Trm induced a mild effect relative to that of HOS. The fitted experimental data for S11, R13, V19, and C48 are shown in Figure 5E. The residues that exhibited high R_2 values in spin relaxation data of the free HBD underwent chemical exchanges on a microsecond-to-millisecond time scale (Figure 5A). We also confirmed that the average ΔR_2^{eff} value of residues S11−F18 (7.43 s^{-1}), which constitutes the Trm-binding site, was decreased upon Trm binding (4.43 s^{-1}). Trm binding has a significant effect on R_{ex} in both N- and C-terminal domains, with the N-terminus affected to a somewhat greater extent. The relaxation dispersions of residues at the C-terminus in HOS-bound HBD, in contrast to those of free HBD and the Trm−HBD complex, almost disappeared (Figure 5C). The average ΔR_2^{eff} value of the free HBD was 4.21 s^{-1}, whereas the corresponding value for the HOS-bound HBD was 2.09 s^{-1}; the corresponding value for the HBD−Trm−HOS complex was 1.69 s^{-1}, implying that the binding of HOS interferes with the slow conformational motions of the HBD and results in global stabilization of the protein conformation. Moreover, the average ΔR_2^{eff} value of residues at the C-terminus (30−55) in the HBD−Trm complex was 3.07 s^{-1}, whereas the corresponding value for the HOS-bound HBD was 1.83 s^{-1}. In particular, dramatic decreases in ΔR_2^{eff} values were observed for R13 (13.08 to 0.75 s^{-1}), R14 (12.70 to 3.23 s^{-1}), N44 (14.90 to 1.88 s^{-1}), C48 (11.46 to 4.62 s^{-1}), and D51 (15.90 to 1.30 s^{-1})

dx.doi.org/10.1021/bi4011682 | Biochemistry 2013, 52, 8823−8832

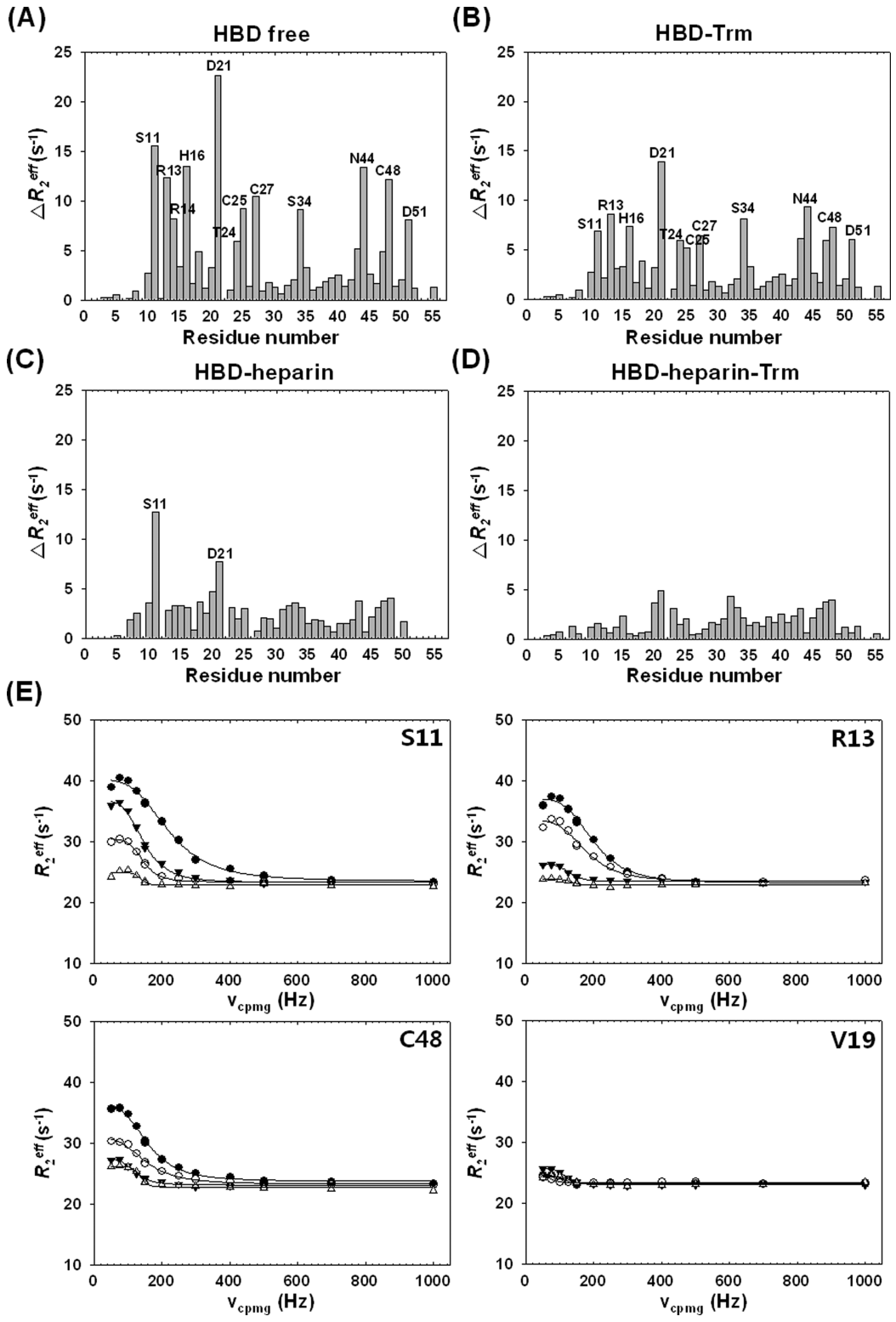

Figure 5. Chemical exchanges in (A) the free HBD and the (B) HBD−Trm, (C) HBD−HOS, and (D) HBD−Trm−HOS complexes. The ΔR_2^{eff} (ν_{cp}) value was determined from the difference in measured relaxation rates, R_2^{eff} (ν_{cp}, 50 Hz) − R_2^{eff} (ν_{cp}, 1000 Hz). (E) Experimental data for the free HBD (●) and the HBD−Trm (○), HBD−HOS (▼), and HBD−Trm−HOS complexes (▽) recorded using 500 MHz NMR. Solid lines indicate fitted curves.

upon HOS binding. Figure 5D shows the R_2^{eff} values of the HBD in complex with both Trm and HOS, revealing an average ΔR_2^{eff} value of 2.09 s^{-1}.

The fitted experimental NMR data at 500 MHz for S11, R13, and H16 are shown in Figure 5E. These residues at the Trm- or HOS-binding site underwent chemical exchange on a microsecond-to-millisecond time scale in the free HBD form. In contrast to those of the free HBD, the level of relaxation dispersion of S11 was dramatically decreased in the Trm-bound form, and those of R13 and C48 were also dramatically

dx.doi.org/10.1021/bi4011682 | *Biochemistry* 2013, 52, 8823−8832

decreased in the HOS-bound form as a result of conformational stabilization. Fitted data for V19 in the nonbinding site, included as a control, showed that the values of R_2^{eff} (ν_{cp}) were invariant to CPMG pulse spacing, indicating that no conformational motion existed on this time scale (Figure 5E). Thus, the relaxation study provided evidence that slow time-scale motions near the ligand-binding site may be important for ligand binding.

Binding Model of HOS and the HBD. It has been reported that positively charged residues in the HBD are critical for heparin binding activity. On the basis of the results obtained from chemical shift perturbation and spin relaxation experiments, we constructed possible models of HBD−HOS and HBD−Trm−HOS complexes, respectively, using docking and MD simulations. When HOS binds to the HBD or HBD−Trm complex, two clustered regions exhibited large chemical shift perturbations. As shown in Figure 2B, each affected region contained positively charged residues: R13, R14, and K15 and K30, R35, and R49, respectively. Also, hNOE values of these residues increased and extents of conformational exchange decreased upon binding of HOS (Figure 4). All HBD atoms were fixed with the exception of the side chains of the residues listed above at the HOS-binding surfaces. In addition, intermolecular NOEs between R13 and H-2 of GlcNS(6S) and R49 and H-5 of GlcNS(6S) were observed, as shown in Figure 6. Therefore, we applied distance constraints (2.5−4 Å)

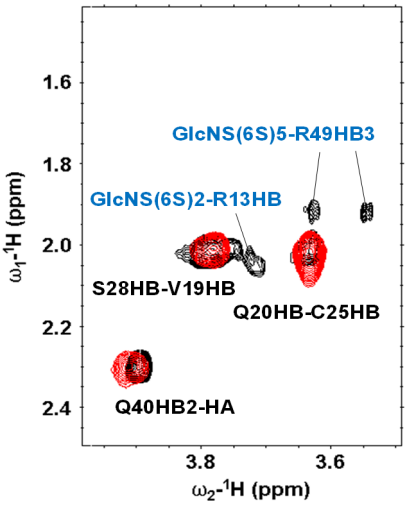

Figure 6. 2D NOESY proton spectrum (500 MHz) of the free HBD (red) and the HBD−HOS complex (black) with a mixing time of 250 ms in 25 mM sodium acetate (pH 5.5) at 300 K. The spectrum is labeled with some NOEs, including intermolecular NOEs (blue) between HOS and the HBD.

for the interactions between side chains of these residues and HOS. The docking model of HOS with the HBD−Trm complex and the specific interactions between HOS and the HBD are shown in panels A and B of Figure 7, respectively. The model of the complex showed that HOS-binding residues in the HBD are clustered on the side opposite the Trm-binding site (Figure 7A). HOS and the HBD interact via hydrogen bonds between the N^{η} atoms of R13, R14, R35, and R49 and N^{ζ} atoms of K30 and the sulfate groups of HOS (Figure 7B). The docking calculation successfully reproduced the expected electrostatic interactions between HOS and the HBD.

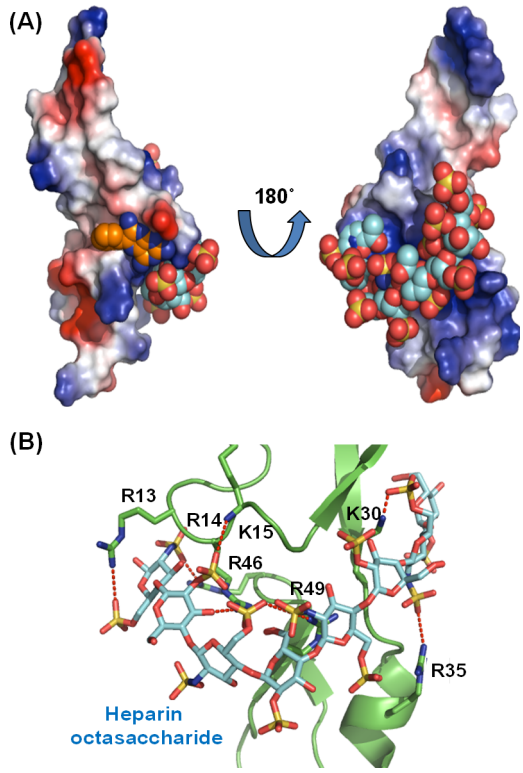

Figure 7. (A) Surface model of the HBD in complex with both Trm (orange) and HOS (cyan) determined by a docking study. (B) Binding model of the HOS and HBD complex showing hydrogen bonds and salt bridges (red dashed lines) involving the backbone amide of K15 and side chains of R13, R14, K30, R35, R46, and R49 with HOS.

DISCUSSION AND CONCLUSIONS

In a previous study, we showed that Trm inhibits VEGF−Aβ interactions without affecting other biological activities of VEGF or Aβ.[27] On the basis of backbone dynamics and a molecular docking study of the HBD and HBD−Trm complex, we suggested that molecular motions in the N-terminal disordered loop region of the HBD are important for interactions with the inhibitor Trm.[27] Interestingly, despite binding Trm, residues in the C-terminal region of the HBD still showed slow motions; therefore, we expected that these C-terminal motions, which are important for biological function, would be recognized by heparin molecules. Here, we modeled binding of HOS to the HBD based on NMR experiments and docking studies. We also investigated the dynamics properties of the HBD in complex with HOS and both HOS and Trm and sought to explain why binding of Trm to the HBD did not affect the biological function of $VEGF_{165}$.

Earlier studies based on docking model and site-directed mutagenesis predicted that the HBD basic residues R13, R14, K30, and R49 are critical for interaction with heparin.[44] Heparin has a very high negative charge density and has regulatory effects on the binding of VEGF to its receptor. Heparin-binding sites should take the form of positively charged pockets. In our NMR experiments, the residues showing large chemical shift perturbations in HSQC spectra are clustered in two regions (Figure 2). Consistent with these data and previous predictions, each affected region includes positively charged residues, R13, R14, and K15 and K30, R35, and R49, respectively. The result of the titration of Trm to the

dx.doi.org/10.1021/bi4011682 | Biochemistry 2013, 52, 8823−8832

HBD−HOS complex also showed chemical shift perturbations in the titration of Trm to the HBD, implying that Trm does not effect the binding of HOS to the HBD.

^{15}N NMR relaxation studies of backbone amides yield hNOE values, large-amplitude motions on nanosecond-to-picosecond time scales, elucidating the conformational dynamics of a protein.[45] Furthermore, slow motions on microsecond-to-millisecond time scales are related to biologically important functional processes, such as ligand docking and protein folding.[46,47] These motions are identified by the R_{ex} term, which indicates exchanges between conformations in various chemical environments. Internal motions within the free HBD and the HBD complexed with ligand have been studied using ^{15}N relaxation techniques.

We have reported that the HBD is a highly mobile protein in which most residues exhibit chemical or conformational exchanges caused by loop motions and isomerization of proline residues and disulfide bonds.[27] However, the binding of HOS to the HBD reduced the local dynamics, and the large R_2 values (>10 s^{-1}) characteristic of certain residues in the free HBD disappeared in the HBD complex with HOS, implying that slow motions are closely related to heparin binding (Figure 4). The R_{ex} at N-terminal loop region was reduced in the presence of Trm and was fully eliminated in presence of both HOS and Trm; this may be important in inhibitor binding as well as Aβ binding. Millisecond-to-microsecond time-scale motions in the HBD were identified using CPMG experiments (see Figure 5). In particular, the R_2^{eff} values of R13, R14, N44, C48, and D51 decreased dramatically upon HOS binding (Figure 5A,C). This predicts that HOS interacts with positively charged side chains of R13 and R14 as well as the C-terminal residue, R49, reducing the extent of conformational exchange near the HOS-binding site of the HBD. The high R_2^{eff} values of residues in the Trm-binding site (S11−F18) also decreased upon Trm binding (Figure 5B). Thus, a comparative study of dynamics features between the free HBD and complexes of the HBD with inhibitor or ligand showed that motions of residues in the binding site may be correlated to inhibitor−ligand binding.

Studies of binding of heparin-derived oligosaccharides to VEGF by Linhardt and co-workers showed that the binding affinity of the oligosaccharide for the HBD increased as the length of the heparin oligosaccharide increased from HOS (4.8 ± 0.4 μM) to hexadecasaccharide (0.48 ± 0.05 μM).[19] N44 is located near the positively charged C-terminal residues R39, R46, and R49. Therefore, we expected that the motion of N44 would reflect the dynamics in its surroundings, and N44 may interact with longer heparin oligosaccharides.

Previously, we showed that Trm inhibits the binding of Aβ to VEGF but does not inhibit the interaction of VEGF with its receptor. We also have reported that motions in the disordered loop region of the N-terminus may be correlated to the binding of Trm. In contrast, C-terminal residues continued to exhibit slow conformational motions, even in the HBD−Trm complex, leading us to conclude that these motions in the C-terminal region might be important for interactions with heparin molecules. In this study, we determined binding models of the HBD or HBD−Trm complex with HOS and investigated slow motions at the C-terminus of the HBD. These modeling studies revealed that the flexible C-terminal region of the HBD plays an important role in the heparin recognition process. As shown in this study, Trm binding has a much stronger effect on intrinsic motions in N-terminal domain than in C-terminal domains, implying that this has a correlation with allowing VEGF to retain its biological function. The information about the structure and dynamic properties of the HBD provided by this study demonstrates that the flexibility of the HBD may be correlated to VEGF function and interaction with inhibitors or other protein partners.

■ ASSOCIATED CONTENT

Ⓢ Supporting Information

Figures S1 and S2. This material is available free of charge via the Internet at http://pubs.acs.org.

■ AUTHOR INFORMATION

Corresponding Author

*Department of Bioscience and Biotechnology, Konkuk University, Seoul 143-701, South Korea. Telephone: +822-450-3421. Fax: +822-447-5987. E-mail: ymkim@konkuk.ac.kr.

Funding

This work was supported by Basic Science Research Program through the National Research Foundation of Korea (NRF), funded by the Ministry of Education (2011-0022873, 2013R1A1A2058021).

Notes

The authors declare no competing financial interest.

■ REFERENCES

(1) Dvorak, H. F., Brown, L. F., Detmar, M., and Dvorak, A. M. (1995) Vascular permeability factor/vascular endothelial growth factor, microvascular hyperpermeability, and angiogenesis. *Am. J. Pathol. 146*, 1029−1039.

(2) Ferrara, N. (1995) The role of vascular endothelial growth factor in pathological angiogenesis. *Breast Cancer Res. Treat. 36*, 127−137.

(3) Carmeliet, P., Ferreira, V., Breier, G., Pollefeyt, S., Kieckens, L., Gertsenstein, M., Fahrig, M., Vandenhoeck, A., Harpal, K., Eberhardt, C., Declercq, C., Pawling, J., Moons, L., Collen, D., Risau, W., and Nagy, A. (1996) Abnormal blood vessel development and lethality in embryos lacking a single VEGF allele. *Nature 380*, 435−439.

(4) Ferrara, N., Carver Moore, K., Chen, H., Dowd, M., Lu, L., O'Shea, K. S., Powell Braxton, L., Hillan, K. J., and Moore, M. W. (1996) Heterozygous embryonic lethality induced by targeted inactivation of the VEGF gene. *Nature 380*, 439−442.

(5) Folkman, J. (1995) Angiogenesis in cancer, vascular, rheumatoid and other disease. *Nat. Med. 1*, 27−31.

(6) Ferrara, N. (2009) Vascular endothelial growth factor: Basic biology and clinical applications. *Current Clinical Oncology 1*, 11−21.

(7) Hoeben, A., Landuyt, B., Highley, M. S., Wildiers, H., Van Oosterom, A. T., and De Bruijn, E. A. (2004) Vascular endothelial growth factor and angiogenesis. *Pharmacol. Rev. 56*, 549−580.

(8) Shweiki, D., Itin, A., Soffer, D., and Keshet, E. (1992) Vascular endothelial growth factor induced by hypoxia may mediate hypoxia-initiated angiogenesis. *Nature 359*, 843−845.

(9) Muller, Y. A., Li, B., Christinger, H. W., Wells, J. A., Cunningham, B. C., and de Vos, A. M. (1997) Vascular endothelial growth factor: Crystal structure and functional mapping of the kinase domain receptor binding site. *Proc. Natl. Acad. Sci. U.S.A. 94*, 7192−7197.

(10) Keyt, B. A., Berleau, L. T., Nguyen, H. V., Chen, H., Heinsohn, H., Vandlen, R., and Ferrara, N. (1996) The carboxyl-terminal domain (111−165) of vascular endothelial growth factor is critical for its mitogenic potency. *J. Biol. Chem. 271*, 7788−7795.

(11) Krilleke, D., Ng, Y. S., and Shima, D. T. (2009) The heparin-binding domain confers diverse functions of VEGF-A in development and disease: A structure-function study. *Biochem. Soc. Trans. 37*, 1201−1206.

(12) Ashikari-Hada, S., Habuchi, H., Kariya, Y., and Kimata, K. (2005) Heparin regulates vascular endothelial growth factor165-dependent mitogenic activity, tube formation, and its receptor

phosphorylation of human endothelial cells. Comparison of the effects of heparin and modified heparins. *J. Biol. Chem. 280*, 31508−31515.
(13) Hamma-Kourbali, Y., Vassy, R., Starzec, A., Le Meuth-Metzinger, V., Oudar, O., Bagheri-Yarmand, R., Perret, G., and Crépin, M. (2001) Vascular endothelial growth factor 165 ($VEGF_{165}$) activities are inhibited by carboxymethyl benzylamide dextran that competes for heparin binding to $VEGF_{165}$ and $VEGF_{165}$ KDR complexes. *J. Biol. Chem. 276*, 39748−39754.
(14) Fairbrother, W. J., Champe, M. A., Christinger, H. W., Keyt, B. A., and Starovasnik, M. A. (1998) Solution structure of the heparin-binding domain of vascular endothelial growth factor. *Structure 15*, 637−648.
(15) Stauffer, M. E., Skelton, N. J., and Fairbrother, W. J. (2002) Refinement of the solution structure of the heparin binding domain of vascular endothelial growth using residual dipolar coupling. *J. Biomol. NMR 23*, 57−61.
(16) Ferro, V., Dredge, K., Liu, L., Hammond, E., Bytheway, I., Li, C., Johnstone, K., Karoli, T., Davis, K., Copeman, E., and Gautam, A. (2007) PI-88 and novel heparan sulfate mimetics inhibit angiogenesis. *Semin. Thromb. Hemostasis 33* (5), 557−562.
(17) Folkman, J., Langer, R., Linhardt, R. J., Haudenschild, C., and Taylor, S. (1983) Angiogenesis inhibition and tumor-regression caused by heparin or heparin fragment in the presence of cortisone. *Science 221* (4612), 719−725.
(18) Mousa, S. A., Feng, X., Xie, J., Du, Y., Hua, Y., He, H., O'Connor, L., and Linhardt, R. J. (2006) Synthetic oligosaccharide stimulates and stabilizes angiogenesis: Structure-function relationships and potential mechanisms. *J. Cardiovasc. Pharmacol. 48* (2), 6−13.
(19) Zhao, W., McCallum, S. A., Xiao, Z., Zhang, F., and Linhardt, R. J. (2012) Binding affinities of vascular endothelial growth factor (VEGF) for heparin-derived oligosaccharides. *Biosci. Rep. 32* (1), 71−81.
(20) Norrby, K., and Nordenhem, A. (2010) Dalteparin, a low-molecular-weight heparin, promotes angiogenesis mediated by heparin-binding VEGF-A in vivo. *APMIS 118* (12), 949−957.
(21) Amirkhosravi, A., Mousa, S. A., Amaya, M., and Francis, J. L. (2003) Antimetastatic effect of tinzaparin, a low-molecular-weight heparin. *J. Thromb. Haemostasis 1* (9), 1972−1976.
(22) Downing, L. J., Strieter, R. M., Kadell, A. M., Wilke, C. A., Greenfield, L. J., and Wakefield, T. W. (1998) Low-dose low-molecular-weight heparin is anti-inflammatory during venous. *Journal of Vascular Surgery 28* (5), 848−854.
(23) Hasan, J., Shnyder, S. D., Clamp, A. R., McGown, A. T., Bicknell, R., Presta, M., Bibby, M., Double, J., Craig, S., Leeming, D., Stevenson, K., Gallagher, J. T., and Jayson, G. C. (2005) HOSs inhibit angiogenesis in vivo. *Clin. Cancer Res. 11* (22), 8172−8179.
(24) Norrby, K. (2000) 2.5 kDa and 5.0 kDa heparin fragments specifically inhibit microvessel sprouting and network formation in $VEGF_{165}$-mediated mammalian angiogenesis. *Int. J. Exp. Pathol. 81* (3), 191−198.
(25) Norrby, K., and Ostergaard, P. (1996) Basic-fibroblast-growth-factor-mediated de novo angiogenesis is more effectively suppressed by low-molecular-weight than by high-molecular-weight heparin. *Int. J. Microcirc. Clin. Exp. 16* (1), 8−15.
(26) Cole, C. L., Hansen, S. U., Baráth, M., Rushton, G., Gardiner, J. M., Avizienyte, E., and Jayson, G. C. (2010) Synthetic heparan sulfate oligosaccharides inhibit endothelial cell functions essential for angiogenesis. *PLoS One 5* (7), No. e11644.
(27) Jeong, K.-W., Lee, J.-Y., Lee, S.-A., Yang, S.-P., Ko, H., Kang, D.-I., Chae, C.-B., and Kim, Y. (2011) Dynamics of a heparin-binding domain of $VEGF_{165}$ complexed with its inhibitor Triamterene. *Biochemistry 50*, 4843−4854.
(28) Bae, D.-G., Gho, Y.-S., Yoon, W.-H., and Chae, C.-B. (2000) Arginine-rich anti-vascular endothelial growth factor peptides inhibit tumor growth and metastasis by blocking angiogenesis. *J. Biol. Chem. 275*, 13588−13596.
(29) Wu, G., Robertson, D. H., Brooks, C. L., III, and Vieth, M. A. (2003) Detailed analysis of grid-based molecular docking: A case study of CDOCKER-A CHARMm-based MD docking algorithm. *J. Comput. Chem. 24*, 1549−1562.
(30) Vieth, M., Hirst, J. D., Kolinski, A., and Brooks, C. L. (1998) Assessing energy functions for flexible docking. *J. Comput. Chem. 19*, 1612−1622.
(31) Vieth, M., Hirst, J. D., Dominy, B. N., Daigler, H., and Brooks, C. L. (1998) Assessing search strategies for flexible docking. *J. Comput. Chem. 19*, 1623−1631.
(32) Mulloy, B., Forster, M. J., Jones, C., and Davies, D. B. (1993) N.m.r. and molecular-modeling studies of the solution conformation of heparin. *Biochem. J. 293*, 849−858.
(33) Marion, D., Driscoll, P. C., Kay, L. E., Wingfield, P. T., Bax, A., Gronenborn, A. M., and Clore, G. M. (1989) Overcoming the overlap problem in the assignment of ^{1}H NMR spectra of larger proteins by use of three-dimensional heteronuclear proton-nitrogen-15 Hartmann-Hahn-multiple quantum coherence and nuclear overhauser-multiple quantum coherence spectroscopy: Application to interleukin 1β. *Biochemistry 28*, 6150−6156.
(34) Cavanagh, J., and Rance, M. (1990) Sensitivity improvement in isotropic mixing (TOCSY) experiments. *J. Magn. Reson. 88*, 72−85.
(35) Kordel, J., Skelton, N. J., Akke, M., Plamer, A. G., III, and Chazin, W. J. (1992) Backbone dynamics of calcium-loaded calbindin D9k studied by two dimensional proton-detected ^{15}N NMR spectroscopy. *Biochemistry 31*, 4856−4866.
(36) Skelton, N. J., Palmer, A. G., III, Akke, M., Kördel, J., Rance, M., and Chazin, W. J. (1993) Practical aspects of two-dimensional proton-detected ^{15}N spin relaxation measurements. *J. Magn. Reson., Ser. B 102*, 253−264.
(37) Kay, L. E., Keifer, P., and Saarinen, T. (1992) Pure absorption gradient enhanced heteronuclear single quantum correlation spectroscopy with improved sensitivity. *J. Am. Chem. Soc. 114*, 10663−10665.
(38) Kempf, J. G., and Loria, J. P. (2003) in *Protein NMR Techniques* (Downing, A. K., Ed.) Humana Press, Totowa, NJ.
(39) Delaglio, F., Grzesiak, S., Vuister, G. W., Zhu, G., Pfeifer, J., and Bax, A. (1995) NMRPipe: A multidimensional spectral processing system based on UNIX pipes. *J. Biomol. NMR 6*, 277−293.
(40) Goddard, T. D., and Kneller, D. G. (2008) *SPARKY 3*, University of California, San Francisco.
(41) Tollinger, M., Skrynnikov, N. R., Mulder, F. A. A., Forman-Kay, J. D., and Kay, L. E. (2001) Slow dynamics in folded and unfolded states of an SH3 domain. *J. Am. Chem. Soc. 123*, 11341−11352.
(42) Mulder, F. A. A., Skrynnikov, N. R., Hon, B., Dahlquist, F. W., and Kay, L. E. (2001) Measurement of slow (μs-ms) time scale dynamics in protein side chains by ^{15}N relaxation dispersion NMR spectroscopy: Application to Asn and Gln residues in a cavity mutant of T4 lysozyme. *J. Am. Chem. Soc. 123*, 967−975.
(43) Robinson, C. J., Mulloy, B., Gallagher, J. T., and Stringer, S. E. (2006) $VEGF_{165}$-binding sites within heparan sulfate encompass two highly sulfated domains and can be liberated by K5 lyase. *J. Biol. Chem. 281* (3), 1731−1740.
(44) Krilleke, D., DeErkenez, A., Schubert, W., Giri, I., Robinson, G. S., Ng, Y. S., and Shima, D. T. (2007) Molecular mapping and functional characterization of the VEGF164 heparin-binding domain. *J. Biol. Chem. 282*, 28045−28056.
(45) Palmer, A. G., III, Williams, J., and McDermott, A. (1996) Nuclear Magnetic Resonance Studies of Biopolymer Dynamics. *J. Phys. Chem. 100* (31), 13293−13310.
(46) Fersht, A. (1985) *Enzyme Structure and Mechanism*, 2nd ed., Freeman & Co., New York.
(47) Jackson, S. E. (1998) How do small single-domain proteins fold? *Folding Des. 3* (4), R81−R91.